Uncertainty in water transit time estimation with StorAge Selection functions and tracer data interpolation

Arianna Borriero[1], Rohini Kumar[2], Tam V. Nguyen[1], Jan H. Fleckenstein[1,3], and Stefanie R. Lutz[4]

[1]Department of Hydrogeology, Helmholtz-Centre for Environmental Research - UFZ, Leipzig, Germany
[2]Department of Computational Hydrosystems, Helmholtz-Centre for Environmental Research - UFZ, Leipzig, Germany
[3]Bayreuth Centre of Ecology and Environmental Research, University of Bayreuth, Bayreuth, Germany
[4]Copernicus Institute of Sustainable Development, Department of Environmental Sciences, Utrecht University, Utrecht, the Netherlands

Correspondence: Arianna Borriero (arianna.borriero@ufz.de)

Abstract. Transit time distributions (TTDs) of streamflow are useful descriptors for understanding flow and solute transport in catchments. Catchment-scale TTDs can be modeled using tracer data (e.g., $\delta^{18}O$; oxygen isotopes) in inflow and outflows, with StorAge Selection (SAS) functions. However, tracer data are often sparse in space and time, so they ~~can~~ need to be interpolated to increase their spatio-temporal resolution. ~~Also~~Moreover, SAS functions can be parameterized with different forms, but there is no general agreement on which one should be used. Both of these aspects induce uncertainty in the simulated TTDs, and the individual uncertainty sources as well as their combined effect have not been fully investigated. This study provides a comprehensive analysis of the TTD uncertainty resulting from twelve model setups obtained by combining different interpolation schemes for $\delta^{18}O$ in precipitation, and distinct SAS functions. ~~Furthermore, we evaluated the value of the young water fraction (F_{yw}) as an additional constraint for the TTD uncertainty.~~ For each model setup, we found behavioral solutions with satisfactory model performances for instream $\delta^{18}O$ (Kling-Gupta Efficiency, KGE>0.57). Differences in KGE values were statistically significant, thus showing the relevance of the chosen setup for simulating the TTDs. We found a large uncertainty in the simulated TTDs, ~~with a 90~~represented by a large range of variability in the 95% confidence interval ~~varying between 286 and 895~~ of the median transit time varying between 259 and 1009 days across all tested setups. Uncertainty in TTDs was mainly associated with the temporal interpolation of $\delta^{18}O$ in precipitation, the choice between time-variant ~~SAS function, and low flow conditions. The use of F_{yw} as an additional constraint substantially reduced the uncertainty in the predicted TTD by up to 49%. We discussed~~ and time-invariant SAS functions, flow conditions, and less with the spatial interpolation methods. We discuss the implications of these results ~~with respect to the study area and the~~ for the SAS framework, ~~in order to identify ways to improve uncertainty characterization and water age simulations~~ uncertainty characterization in TTD-based models, and the influence of the uncertainty for water quality and quantity studies.

1 Introduction

Understanding how catchments store and release water of different ages has significant implications for flow and solute transport as water ages encapsulate information about flowpaths characteristics (McGuire and McDonnel, 2006; Botter et al., 2011),

contact time of solutes with the soil matrix (Benettin et al., 2015a; Hrachowitz et al., 2016), and vulnerability assessment (Kumar et al., 2020). This plays an important role for water resources protection and management, ~~as well as~~ and requires a tool that can effectively describe catchment-scale transport processes (Rinaldo and Marani, 1987). The ~~water age~~ age of water in outflows is commonly referred to as transit time (TT), i.e., the time elapsed between the entry of a water parcel into the catchment via precipitation and its exit via streamflow or evapotranspiration. Accordingly, the transit time distribution (TTD) describes the whole spectrum of the transit times in outflows (Botter et al., 2005; Van der Velde et al., 2010). Early studies have often assumed simplified steady-state transport models, resulting in time-invariant TTDs (Niemi, 1977; Rinaldo et al., 2006). However, experimental simulations showed that TTDs are time-variant due to the variability in meteorological forcing (Botter et al., 2010; Hrachowitz et al., 2010; Heidbüchel et al., 2020) ~~. A promising tool~~ and activation/deactivation of flowpaths in response to varying hydrologic conditions (Ambroise, 2004; Heidbüchel et al., 2013). Recent research has introduced new models for representing time-variant TTDs~~are StorAge Selection~~ , for example allowing for the estimation of TTDs without making prior assumptions about their shape (Kirchner, 2019; Kim and Troch, 2022), or via parameterization of the StorAge Selections (SAS) functions ~~, which~~ (Rinaldo et al., 2015; Harman, 2019). SAS functions describe how catchments selectively remove water of different ages from storage ~~to outflows(Rinaldo et al., 2015; Harman, 2019). SAS functions~~ for outflows, and have led to a new framework of non-stationary transport models based on water age, which have been successfully applied in various transport modelling studies (Benettin et al., 2015b; Queloz et al., 2015; Kim et al., 2016; Lutz et al., 2017; Wilusz et al., 2017; Nguyen et al., 2021).

Model-based TTDs are subjected to uncertainty, which limits their ability for decision support. In general, model prediction uncertainty stems from model inputs, structure, and parameters (Beven and Freer, 2001). As TTDs are not directly observable, conservative environmental tracers (e.g., $\delta^{18}O$; oxygen isotopes) in inflow and outflows are commonly used to infer water ages (Hrachowitz et al., 2013; Birkel and Soulsby, 2015; Stockinger et al., 2015). Long-term, high-frequency tracer data with ~~an~~ appropriate spatial distribution are generally recommended for sufficient understanding of ~~the TTDs~~ TTD dynamics across a wide range of fast and heterogeneous hydrological behaviors (Kirchner et al., 2004; Danesh-Yazdi et al., 2016; von Freyberg et al., 2017). Therefore, the lack of ~~an~~ appropriate tracer data coverage can ~~prevent~~ hamper our understanding of ~~the TTDs~~ TTD dynamics at the desired resolution (McGuire and McDonnel, 2006). Additionally, uncertainty in the driving hydroclimatic fluxes such as precipitation, discharge, and evapotranspiration could propagate into the uncertainty of the modelling results. Further uncertainty emerges from the model structure due to the difficulty in representing physical processes because of our incomplete knowledge of complex reality (Ajami et al., 2007). Finally, specification of model parameters is also an important source of uncertainty (Beven, 2006; Kirchner, 2006), as the best-fit parameters may suffer from equifinality (Schoups et al., 2008).

A few studies have investigated the uncertainty in the estimated TTDs with SAS models. Danesh-Yazdi et al. (2018) and Jing et al. (2019) have analysed the effect of ~~the~~ interactions between distinct flow domains, external forcing and recharge rate on resulting TTDs. Several works (Benettin et al., 2017; Wilusz et al., 2017; Rodriguez et al., 2018, 2021) have explored model parameter uncertainty, and suggested that additional types of tracers, data on physical characteristics of the catchment, and parsimonious parameterization may help to further reduce ~~parameters uncertainty~~ parametric uncertainty in the SAS modelling

approach. More recently, Buzacott et al. (2020) investigated how gap-filling of the $\delta^{18}O$ record in precipitation propagated uncertainty into the simulated mean water transit time (MTT), i.e., the average time it takes for water to leave the catchment (McDonnel et al., 2010).

Despite the studies cited above, there are other aspects particularly significant for SAS modelling causing uncertainty in the simulated TTDs, which have not yet been ~~fully addressed~~thoroughly investigated. First, isotope data are generally sparse globally in space and time (von Freyberg et al., 2022), due to laborious and costly sampling campaigns limited to well-equipped areas (Tetzlaff et al., 2018). ~~For this reason, spatio-temporal interpolation of the isotope composition in precipitationcan be used to get greater data coverage, required for modelling purposes. Second,~~ As SAS models require continuous time series of input tracer data, different methods for temporal interpolation could be used to fill gaps in isotope values in precipitation; consequently, the interpolated input data are subject to uncertainty. Furthermore, the input data of SAS models are influenced by whether the tracer data in precipitation are collected at a single location within the catchment, or at multiple locations. In the latter scenario, there is a need to account for the spatial variability of tracer composition in precipitation, which is commonly done via spatial interpolation. Choosing data from one approach (i.e., tracer data from a single location) over the other (i.e., multiple tracer data spatially interpolated) can potentially result in different resulting TTDs. Finally, SAS functions, employed to model TTDs, must be parameterized and ~~commonly used parameterizations~~ their functional forms need to be specified a-priori. Commonly used forms are the power law (Benettin et al., 2017; Asadollahi et al., 2020), beta (van der Velde et al., 2012; Drever and Hrachowitz, 2017) ~~distribution~~and gamma (Harman, 2015; Wilusz et al., 2017) distributions. However, there is no general agreement on which SAS function should be used ~~as~~ since the hydrological processes ~~which control subsurface mixing, hence TTDs dynamics , are distinct across different~~ that control the patterns and dynamics of the subsurface vary across catchments. Therefore, the most convenient approach is to simply rely on ~~one~~ a specific parameterization over another, and estimate its parameters (Harman, 2015). ~~Both~~ All of these aspects~~induce~~ , related to model input, structure and parameter, induce uncertainty in the simulated TTDs. To date, the role of these individual uncertainty sources and their combined effect on the modeled TTDs have not been adequately discussed.

~~To reduce the estimated TTD uncertainty, various studies have suggested combining stable and decaying tracers (Duvert et al., 2016), the latter best imparting old water ages. Others have proposed high sampling resolution (e.g., daily) to provide better insights into short-term events (Timbe et al., 2015). One such example is the young water fraction (F_{yw}; streamflow ratio younger than 2-3 months (Kirchner, 2016a)), which can be easily retrieved from low frequency tracer data covering relatively short period. The estimation of F_{yw} is based on the amplitude ratio of the seasonal cycles in stable water isotopes in precipitation and streamflow. F_{yw} represents an alternative descriptor for TTD, a robust metric under both spatially heterogeneous and non-stationary conditions, as well as less prone to a large aggregation bias than MTTs (Kirchner, 2016b). Benettin et al. (2017) proposed to use F_{yw} to restrict model parameter values, while Lutz et al. (2018) implemented it as an additional constraint in the calibration of gamma-distributed TTDs. However, to the best of our knowledge, no studies have attempted to employ F_{yw} for constraining predictive uncertainties in SAS-based TTDs.~~

This study bridges the aforementioned gaps by specifically exploring the combined effect of sparse input tracer data and model parameterizations on the simulated TTDs. We investigated TTD uncertainty using a SAS-based catchment-scale trans-

port model applied to the Upper Selke catchment, Germany. We evaluated TTDs resulting from twelve model setups obtained by combining distinct interpolation techniques of $\delta^{18}O$ in precipitation, and parameterizations of SAS functions. For each model setup, we searched for behavioral parameter sets (i.e., those providing acceptable predictions) based on model performance for instream $\delta^{18}O$~~. Afterwards, we~~ , and evaluated the sources of uncertainty, as well as their combined effects, in the ~~resulting TTDsand, finally, we tested whether and to what extent F_{yw} could provide valuable information to further constrain the uncertainty~~modeled TTDs. Overall, our results provide new insights into the uncertainty characterization of TTDs, particularly in the absence of high-frequency tracer data, and the use of SAS functions, as well as implications of TTDs uncertainty on water quantity and quality studies.

2 Study area and data

The Upper Selke catchment is located in the Harz Mountains in Saxony-Anhalt, central Germany (Fig. 1). The study site is part of the Bode region, an intensively monitored area within the TERENO (TERrestrial ENvironmental Observatories; Wollschläger et al., 2017) network. The catchment has a drainage area of 184 km^2, the altitude ranges between 184 and 594 m above mean sea level, and the mean slope is 7.65%. Land use is dominated by forest (broadleaf, coniferous and mixed forest) and agricultural land (winter cereals, rapeseed and maize), representing 72% and 21% of the catchment, respectively. The soil is largely composed of cambisols and the underlying geology consists of schist and claystone, resulting in a predominance of relatively shallow flowpaths (Dupas et al., 2017; Yang, J. et al., 2018).

Daily hydroclimatic and monthly tracer data in the Upper Selke were available for the period between February 2013 and May 2015. Precipitation (P) was taken from the German weather service, while discharge (Q) and evapotranspiration (ET) were simulated data obtained from the mesoscale Hydrological Model (mHM; (Samaniego et al., 2010; Kumar et al., 2013)) since continuous measurements were not available for the given outlet and period. A thorough evaluation of mHM performance for past measurements have been conducted in previous studies (Zink et al., 2017; Yang, X. et al., 2018; Nguyen et al., 2021). The average annual P, Q and ET are 703, 108, 596 mm, respectively. The area is characterized by high flow during November-May (average Q = 0.88 m^3/s) and low flow during June-October (average Q = 0.42 m^3/s). Evapotranspiration is higher in June (109 mm/month) and lower in December (10 mm/month). The average monthly temperature ranges from -0.7°C in January to 17°C in July. The $\delta^{18}O$ values in precipitation ($\delta^{18}O_P$) and in streamflow ($\delta^{18}O_Q$) at monthly resolution were taken from Lutz et al. (2018) (Fig. S1). Values of $\delta^{18}O_P$ were used in the form of "raw" (i.e., values collected at the catchment outlet) and processed (i.e., values collected at multiple location and spatially interpolated using kriging) data (see Section 3.2 for more details). The variability in $\delta^{18}O_P$ was larger than $\delta^{18}O_Q$ (Fig. S1) because of the ~~damped~~ damping of the precipitation signal due to mixing and dispersion within the catchment. Temperature dependence caused more depleted (i.e., more negative) $\delta^{18}O_P$ in winter than in summer (Fig. S1).

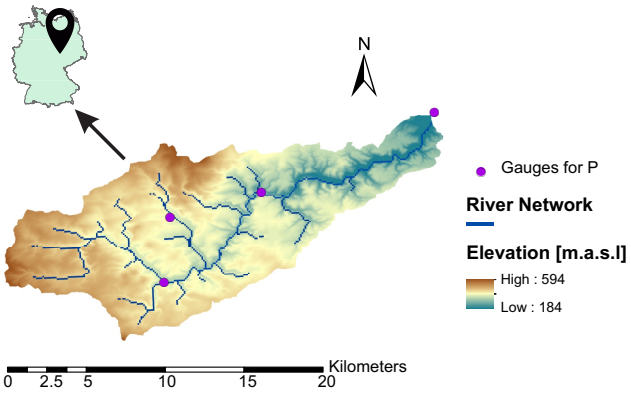

Figure 1. Upper Selke catchment with precipitation sampling points (purple dots), river network (blue lines), and elevation in meters above sea level as colored map; location of the Upper Selke catchment in Germany (upper left corner).

3 Methods

3.1 Catchment-scale transport model

In this study, we used the *tran-SAS* model (Benettin and Bertuzzo, 2018) for describing the catchment-scale water mixing and solute transport based on SAS functions. The catchment was conceptualized as a single storage *S(t)* (mm), whose water-age balance can be expressed as follows (Benettin and Bertuzzo, 2018):

$$S(t) = S_0 + V(t) \tag{1}$$

$$\frac{\partial S_T(T,t)}{\partial t} + \frac{\partial S_T(T,t)}{\partial T} = P(t) - Q(t)\cdot\Omega_Q(S_T,t) - ET(t)\cdot\Omega_{ET}(S_T,t) \tag{2}$$

$$\text{Initial condition: } S_{\mathrm{T}}(T, t=0) = S_{\mathrm{T_0}}(T) \tag{3}$$

$$\text{Boundary condition: } S_{\mathrm{T}}(0,t) = 0 \tag{4}$$

where S_0 (mm) ~~are~~ is the initial storage, *V(t)* (mm) are the storage variations, *P(t)* (mm/d), *Q(t)* (mm/d), and *ET(t)* (mm/d) are precipitation, discharge and evapotranspiration, respectively, $S_T(T,t)$ (mm) is the age-ranked storage, $S_{T0}(T)$ (mm) is the initial age-ranked storage, and $\Omega_Q(S_T,t)$ (-) and $\Omega_{ET}(S_T,t)$ (-) are the cumulative SAS functions for *Q* and *ET*, respectively.

By definition, the TTD of streamflow $p_Q(T,t)$ (d^{-1}) is calculated as follows (Benettin and Bertuzzo, 2018):

$$p_Q(T,t) = \frac{\partial \Omega_Q(S_T,t)}{\partial S_T}\cdot\frac{\partial S_T}{\partial T}. \tag{5}$$

The isotopic signature in streamflow $C_Q(t)$ (‰) can be obtained from (Benettin and Bertuzzo, 2018):

$$C_Q(t) = \int_0^{+\infty} C_S(T,t) \cdot p_Q(T,t) \cdot dT \tag{6}$$

where $C_S(T,t)$ (‰) is the isotopic signature of a water parcel in storage. Equations 5 and 6 also apply for *ET*.

In this study, we tested three SAS parameterizations: the power law time-invariant (PLTI; Eq. 7 (Queloz et al., 2015)), power law time-variant (PLTV; Eq. 8 (Benettin et al., 2017)), and time-invariant beta ~~distribution (BETA~~(BETATI); Eq. 9 (Drever and Hrachowitz, 2017)) distribution. Here, they are expressed as probability density functions in terms of the normalized age-ranked storage $P_S(T,t)$ (-), also known as fractional SAS functions (fSAS):

$$\omega(P_S(T,t),t) = k \cdot (P_S(T,t))^{k-1} \tag{7}$$

$$\omega(P_S(T,t),t) = k(t) \cdot (P_S(T,t))^{k(t)-1} \tag{8}$$

$$\omega(P_S(T,t),t) = \frac{(P_S(T,t))^{\alpha-1} \cdot (1-P_S(T,t))^{\beta-1}}{B(\alpha,\beta)}. \tag{9}$$

The parameters k, α and β determine the catchment's water age preference for ~~outflow~~outflows, while $B(\alpha,\beta)$ is the two-parameter beta function. If k<1, or if α<1 and β>1, the system tends to discharge young water. If k>1, or if α>1 and β<1, the catchment preferably releases old water. The case of k=1 or α=β=1 describes no selection preference (i.e., complete water mixing). PLTV is characterized by $k(t)$ varying linearly over time between two extremes k_1 and k_2 as a function of the catchment wetness wi (-), i.e., $wi(t) = (S(t)-S_{min})/(S_{max}-S_{min}))$, where S_{min} and S_{max} are the minimum and maximum storage values over the entire period.

3.2 Interpolation techniques for δ^{18}O in precipitation

We tested the model with two spatial and two temporal interpolation methods of tracer data to explore the TTD uncertainty resulting from model input. To evaluate the effect of the spatial interpolation, we first set a base case using monthly raw $\delta^{18}O_P$ taken from Lutz et al. (2018), corresponding to the values collected at ~~the catchment outlet (~~a single location, i.e. ~~, Meisdorf station)~~the catchment outlet at Meisdorf station. Second, we used the spatially interpolated $\delta^{18}O_P$ estimates from Lutz et al. (2018), which are based on raw observations from 24 precipitation collectors spread over the larger area of the Bode region. The spatial interpolation in Lutz et al. (2018) was conducted using kriging with altitude as an external drift. The kriged $\delta^{18}O_P$ were further weighted with spatially distributed monthly precipitation to obtain representative estimates for the study region.

SAS model results are sensitive to the choice of the temporal resolution of input tracer data, and shorter time steps are generally recommended to achieve a satisfactory level of detail (Benettin and Bertuzzo, 2018). Additionally, a forward Euler scheme was employed to solve Eq. 2, whose precision increases with high frequency time steps. For ~~this reason~~these reasons, we reconstructed daily $\delta^{18}O_P$ estimates from monthly values with two different interpolation schemes. First, we used a step function in which the values between two consecutive samples assumed the value of the last sample. Second, we used a sine interpolation based on the assumption that ~~the~~ $\delta^{18}O_P$ values follow a seasonal cycle (Fig. S1 in the Supplement, (Feng et al.,

2009)), whose signature over a period of one year can be described by (Kirchner, 2016a):

$$\delta^{18}O_P(t) = a_P \cdot cos(2 \cdot \pi \cdot f \cdot t) + b_P \cdot sin(2 \cdot \pi \cdot f \cdot t) + k_P \quad (10)$$

where a and b are regression coefficients (-), t is the time (decimal years), f is the frequency (yr^{-1}) and k (‰) is the vertical offset of the isotope signal (‰). The coefficients a and b were estimated by fitting Eq. 10 to monthly $\delta^{18}O_P$ values using the iteratively re-weighted least squares (IRLS) estimation (von Freyberg et al., 2018). Subsequently, the estimated regression coefficients were used in Eq. 10 to obtain isotope data at daily frequency. Figure S2 in the Supplement displays the simulated kriged and raw $\delta^{18}O_P$ values via step function and sine interpolation.

3.3 Estimation of the young water fraction (F_{yw})

F_{yw} was estimated through a sine-wave fit, which assumes that the seasonal cycle in $\delta^{18}O_P$ is transmitted into $\delta^{18}O_Q$ as a damped and phase-shifted signal (Soulsby et al., 2006). In line with (Bliss, 1970), the isotopic signal for $\delta^{18}O_P$ and $\delta^{18}O_Q$ over a year can be written respectively as Kirchner (2016a):

$$c_P(t) = A_P \cdot sin(2 \cdot \pi \cdot f \cdot t - \phi_P) + k_P$$

$$c_Q(t) = A_Q \cdot sin(2 \cdot \pi \cdot f \cdot t - \phi_Q) + k_Q$$

where A is the tracer cycle amplitude (‰), ϕ is the phase of the cycle (radians), t is the time (decimal years), f is the frequency (yr^{-1}) and k (‰) is the vertical offset of the isotope signal. The amplitude ratio defines the young water fraction F_{yw} (Kirchner, 2016a):

$$F_{yw}^{est} = \frac{A_q}{A_p}.$$

A_P and A_Q were calculated with the IRLS method by fitting Eqs. 11 and 11 to monthly $\delta^{18}O_P$ and $\delta^{18}O_Q$ samples volume-weighted with the corresponding P and Q rates; thus, the flow-weighted F_{yw}^{est} was computed (von Freyberg et al., 2018). Gaussian error propagation was applied to assess the standard error (± SE) of F_{yw}^{est} as an uncertainty measure.

This tracer-based F_{yw}^{est} was compared with the simulated young water fraction F_{yw}^{sim} obtained via the SAS model. To determine F_{yw}^{sim}, we averaged the TTDs computed at any time step; then, we flow-weighted the averaged TTDs to obtain the long-term TTD over the entire study period, also known as marginal TTD (Heidbüchel et al., 2012). From the marginal TTD, we computed F_{yw}^{sim} as:

$$F_{yw}^{sim} = P_Q(T = \tau_{yw}).$$

where τ_{yw} is the threshold age set to 75 days, which falls within 2-3 months defining F_{yw} (Kirchner, 2016a). We used F_{yw}^{est} ±SE instead of a specific value to account for the uncertainty associated with a fixed threshold age of τ_{yw}=75 days for F_{yw}^{sim}.

3.3 Experimental design

In this study, different scenarios were used to quantify uncertainty in the modeled results. We tested twelve setups composed of three SAS functions (PLTI, PLTV, ~~BETA~~BETATI), two temporal (step and sine function) and two spatial (raw and kriging values) interpolation techniques (Table 1). For each setup, we performed a ~~Monte Carlo~~ Monte-Carlo experiment by running the model with 10,000 parameter sets generated by the Latin Hypercube Sampling (LHS, McKay et al., 1979). Model parameters and their search ranges are shown in Table 2.

Table 1. List of model setups.

setup	interpolation	SAS function
~~1~~ a	step function kriged $\delta^{18}O_P$	PLTI
~~2~~ b		PLTV
~~3~~ c		~~BETA~~ BETATI
~~4~~ d	step function raw $\delta^{18}O_P$	PLTI
~~5~~ e		PLTV
~~6~~ f		~~BETA~~ BETATI
~~7~~ g	sine function kriged $\delta^{18}O_P$	PLTI
~~8~~ h		PLTV
~~9~~ i		~~BETA~~ BETATI
~~10~~ j	sine function raw $\delta^{18}O_P$	PLTI
~~11~~ k		PLTV
~~12~~ l		~~BETA~~ BETATI

Table 2. Model parameters and search ranges.

SAS parameter	Symbol	Unit	Lower Bound	Upper Bound
~~Discharge SAS parameter~~	k_Q	[-]	0.1	2
~~Discharge SAS parameter~~	k_{Q1} ~~or α~~	[-]	0.1	2
Discharge SAS parameter	k_{Q2} ~~or~~	[-]	0.1	2
	α	[-]	0.1	2
	β	[-]	0.1	2
Evapotranspiration SAS parameter	k_{ET}	[-]	0.1	2
Initial storage	S_0	[mm]	300	3000

A 5 years warm-up period (i.e., repetition of the input data) from February 2008 to January 2013 was performed to reduce the impact of the model initialization. The period from February 2013 to May 2015 was used to infer behavioral model parameters (i.e., parameter sets giving acceptable predictions), and subsequently to interpret the model results. The initial concentration of $\delta^{18}O$ in storage was set to 9.2 ‰ coinciding with the mean $\delta^{18}O_Q$ over the study period.

The ~~generalized likelihood uncertainty estimation (GLUE Beven and Binley, 1992)~~ informal likelihood of the Sequential Uncertainty Fitting Procedure (SUFI-2, Abbaspour et al., 2004) was applied to ~~determine the behavioral parameter sets in terms of the~~ account for uncertainty in the SAS parameter sets and resulting modeled estimates. In SUFI-2, the uncertainty in model parameters and simulated results is represented by a uniform distribution, which is gradually reduced until a specific

criterion is reached. In our study, we calibrated the values of model parameters until the predicted output matched the measured tracer data to a satisfactory level, defined by an objective function. We employed as objective function the Kling-Gupta efficiency (KGE, Gupta et al., 2009)~~for observed and simulated $\delta^{18}O_Q$ values. The best 5% parameter sets were selected as behavioral, from which we constructed the 90% confidence intervals (CI) to refine limits of the~~ , and once the criterion of KGE≥0.5 was satisfied, we defined a set of behavioral solutions for ~~every output variable. Instead of fixing a threshold limit based on KGE, we set the sample size to allow for comparability of the results across different model setups.~~ each model setup. However, since the aim of this study is to investigate the impact of various sources of uncertainty on simulated outputs, rather than to determine the best model setup based on the model efficiency, we decided to set a fixed sample size and narrow down those solutions generated by SUFI-2 in the previous step. Setting a fixed sample size ensures comparability of results across the twelve tested setups, as different sample sizes could influence the uncertainty analysis. For example, the greater the number of behavioral solutions, the wider the uncertainty band. At the same time, by fixing the sample size, we can still meet the requirement of a minimum acceptable KGE value (i.e., KGE≥0.5).

~~From the daily TTDs, we extracted the temporal evolution of the daily~~ In this study, we determined the final behavioral solutions by using a fixed sample size that corresponds to the best 5% parameter sets and modeled results in terms of KGE. Finally, we constructed the 95% confidence intervals (CI) based on the 2.5% and 97.5% CIs of the cumulative distribution in the time series of parameters and output variables (Abbaspour et al., 2004) to refine the limits of the behavioral solutions. In our experimental setup, the main output variables were the instream $\delta^{18}O$ signature and backward median transit time (TT_{50} (days), i.e., the maximum time elapsed until the youngest 50% of the infiltrated water is transferred to the outflow)~~, and used it~~ . Time series of TT_{50} were extracted directly from daily TTDs (Eq. 5) and used as a metric for the streamflow age. This was done because TTDs are typically skewed with long tails (Kirchner et al., 2001)~~; hence,~~ , hence the median is often ~~more suitable~~ a more suitable metric than, for example, MTT as it is less impacted by the poor identifiability of the older water components (Benettin et al., 2017).

~~In a final step, the behavioral parameter sets identified via GLUE were further constrained with F_{yw}^{est}; the behavioral solutions providing F_{yw}^{sim} (Eq. **??**) within the range $F_{yw}^{est} \pm SE$ (Eq. **??**) were chosen as the final behavioral solutions.~~

4 Results

4.1 Simulated $\delta^{18}O$ in streamflow and model performances

Modeled $\delta^{18}O$ in streamflow ($\delta^{18}O_Q$) represented by the ~~90~~95% confidence interval (CI) in the ensemble solution are displayed in Fig. 2. The results reveal how the predicted $\delta^{18}O_Q$ values enveloped the measured isotopic signature by reproducing its seasonal fluctuations, with depleted (i.e., more negative) values in winter and enriched (i.e., ~~more positive~~less negative) values in summer. However, the second half of the study period ~~is~~ was characterized by more enriched predicted $\delta^{18}O_Q$ values than the measured ones. Although the behavioral parameter sets ~~are~~ were able to capture the seasonal isotopic trend, they poorly reproduced the exact values; therefore, the ensemble simulations are characterized by a non-negligible uncertainty.

Figure 2 shows the distinct effects of the interpolated input tracer data and model parameterization on the simulated $\delta^{18}O_Q$ values. The step function interpolation generated an erratic isotopic signature in streamflow with flashy fluctuations, explicitly visible in Fig. 2c and f. On the other hand, the sine interpolation of $\delta^{18}O_P$ values yielded a smooth response in the simulated $\delta^{18}O_Q$ values (Fig. 2g-l). The sine interpolation also induced larger seasonal tracer cycle amplitudes (Fig. 2g-l) than those produced when using the step function (Fig. 2a-f). Conversely, no clear visual difference was found between ~~the raw~~ kriged (Fig. 2~~d-f and j-l) and kriged~~ a-c and g-i) and raw (Fig. 2~~a-c and g-i~~d-f and j-l) $\delta^{18}O_P$ samples as their general patterns match (Fig.~~2S~~ S2 in the Supplement). Likewise, distinct SAS parameterizations ~~produced~~ did not produce remarkable differences in the simulated $\delta^{18}O_Q$ values~~. BETA induced a large 90% CI in the $\delta^{18}O_Q$ values (Fig. 2c, f, i and l), and wide tracer cycle amplitudes. In contrast, both PLTI and PLTV (Fig. 2a, b, d, e, g, h , j~~ , although PLTV generally yielded simulations that better enveloped the measured isotopic signature (Figs. 2b, e, h and k)~~produced a substantially narrow 90% CI with small amplitudes of the simulated $\delta^{18}O_Q$ values~~.

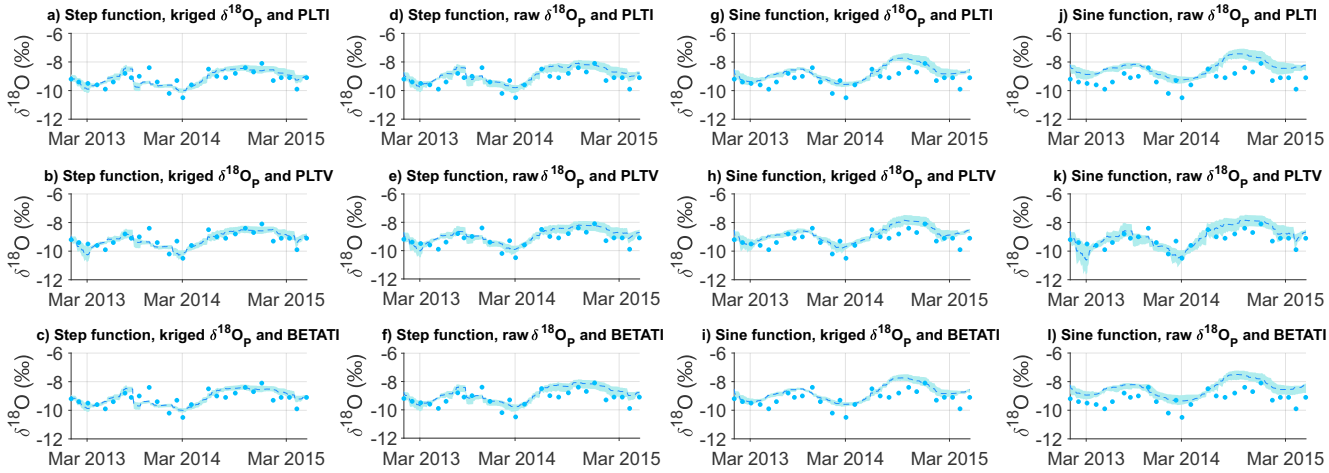

Figure 2. Predicted $\delta^{18}O$ values in streamflow~~identified by 5% best KGE~~. Dark blue filled circles represent the observed data; the light blue line and the shaded area represent, respectively, the ensemble mean of all possible solutions and ~~its variation~~ their range according to the ~~90~~95% CI.

Despite the differences in the predicted $\delta^{18}O_Q$ values, all simulations can be considered satisfactory given the KGE values ranging between 0.57 and 0.75, across all tested setups (Fig. 3). These performances can be classified from intermediate (Thiemig et al., 2013) to good (Andersson et al., 2017; Sutanudjaja et al., 2018). When considering the best fit, the combination of the step function interpolation and raw $\delta^{18}O_P$ values performed best. Additionally, PLTV generally yielded slightly better KGE values than PLTI and ~~BETA~~ BETATI when grouping the setups with the same interpolation ~~techniques~~ technique of $\delta^{18}O_P$. Differences in the ~~KGE means~~ mean KGEs were statistically insignificant (t-test with p-values > 0.05) between setups ~~1 and 3, as well as among setups 6, 7 and 9~~ h and i (Table 1), and this largely ~~matches our visual analysis .~~ agrees with the visual analysis (Fig. 3). Contrarily, the differences in the mean KGE values of the remaining setups were statistically significant (p-values < 0.05), indicating that a priori methodological ~~choices~~ choice (i.e., interpolation techniques of $\delta^{18}O_P$ values and/or SAS

parameterization) strongly impact on the overall results. ~~Notwithstanding~~Nonetheless, this does not mean that we can clearly identify the most suitable setup, but there is need to carefully analyze the multiple potential choices in SAS parameterization and tracer data interpolations, and to evaluate the uncertainty range in modeled predictions.

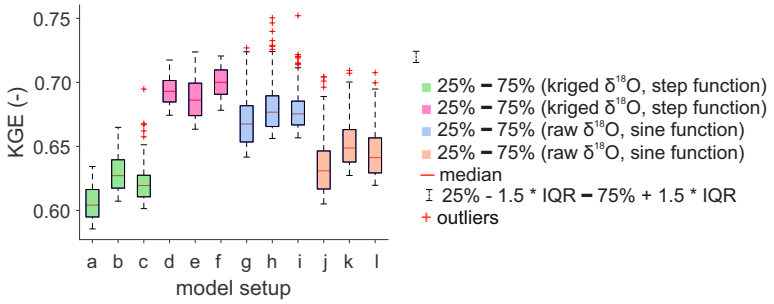

Figure 3. Boxplot of model performance ranges in behavioral solutions~~obtained with 5% best KGE; boxplots~~. The letters on the x-axis refer to the model setup type according to Table 1. Boxplots filled with the same colors represent model setups characterized by the same interpolation scheme in space and time. On each box, the central ~~mark~~ red line indicates the median, and the bottom and top edges of the box indicate the 25th and 75th percentiles ~~,~~ respectively, namely the interquartile range (IQR). The whiskers extend to the most extreme data points not considered outliers ~~,~~ which are 25th percentile minus 1.5 times IQR and ~~the~~ 25th percentile plus 1.5 times IQR, respectively. The outliers are plotted individually using the red '+' mark.

Ranges of the behavioral SAS parameters for the tested setups are summarized in Table S1 in the Supplement. Parameters for the SAS functions of Q (i.e., k_Q, k_{Q1}, k_{Q2}, α and β) were different across the setups although, in general, they were relatively narrow and well identified. However, the behavioral parameters were better constrained when using the step function interpolation since their ~~range~~ 95% CI was, on average, ~~34~~26% narrower than that provided by the sine interpolation, across all the SAS parameterizations. The parameters k_{Q1} and α were also better identified than k_{Q2} and β, since their ~~range~~ 95% CI was, on average, ~~22~~67% narrower, ~~in~~ across all tested setups. Conversely, there was no ~~significant~~ clear difference in the parameters ranges when using kriged or raw $\delta^{18}O_P$ values. The evapotranspiration parameter (i.e., k_{ET}) was poorly identified in all setups as any value in the search range provided equally good results. The initial storage (i.e., S_0) was only partially constrained as any value between ~~400 mm and 2340~~ 340 mm and 2895 mm was considered acceptable.

4.2 Simulated transit times and model uncertainty

Figure 4 illustrates the ~~90~~95% CI of the behavioral solutions for the predicted median transit ~~times~~ time (TT_{50}). The results show that the model ~~simulates very~~ simulated largely different ranges of TT_{50} ~~values~~ based on the tested setups. When using PLTI and ~~BETA, the 90~~BETATI, the 95% CI was relatively stable with small fluctuations throughout the simulation period, compared to PLTV (Fig. 4a, c, d, f, g, i, j and l). However, minor differences emerged across the simulated TT_{50} ~~,~~ as a result of the distinct interpolation techniques used for $\delta^{18}O_P$ ~~values. The 90% CI~~. The 95% CI of TT_{50} was on average ~~slightly larger by 11~~larger by 36%, across all tested setups, when using ~~kriged~~ raw $\delta^{18}O_P$ (Fig. 4~~a-c and g-i~~d-f and j-l) rather than ~~raw~~ kriged $\delta^{18}O_P$ ~~values~~ (Fig. 4~~d-f and j-l). Also, the use of the~~ a-c and g-i). This was especially visible when the step function was used (Fig. 4a-f). Moreover, the sine function generated a ~~90% CI~~ 95% CI of TT_{50} being on average ~~22~~62% narrower across all

tested setups ~~,~~ (Fig. 4g-l) with respect to the step function (Fig. 4a-f)~~, notably within~~ . These differences were more evident for high flow conditions. In addition, the behavioral solutions obtained with ~~BETA~~ the sine function (Fig. 4g-l) were more skewed towards shorter mean TT_{50} values, across all tested setups, ~~in contrast to PLTI and PLTV~~ than those of the step function (Fig. 4~~e, f, i and l~~a-f).

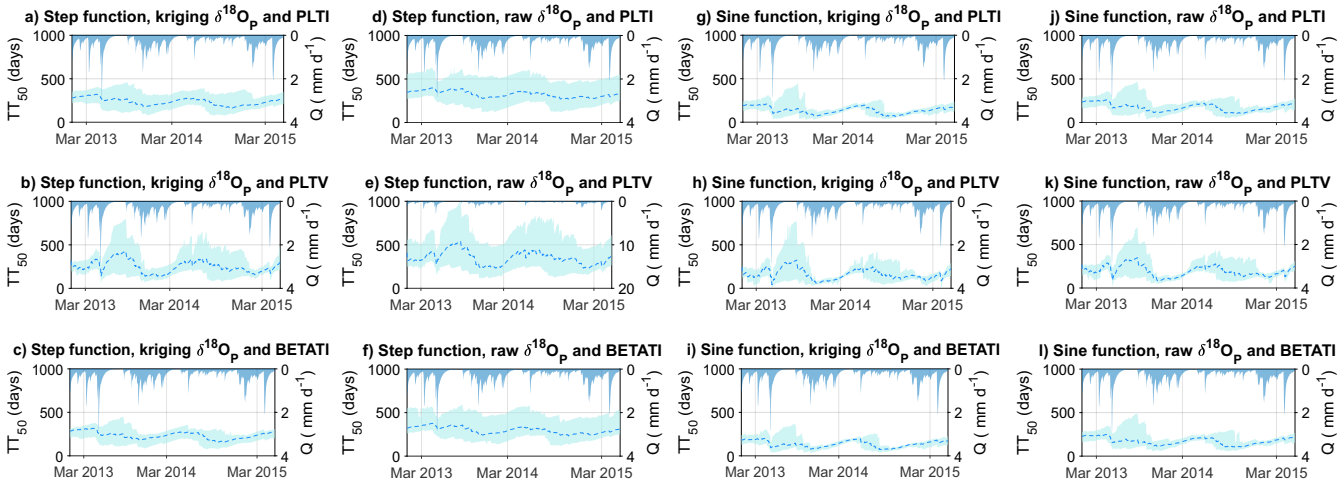

Figure 4. Predicted TT_{50} of streamflow~~identified by 5% best KGE~~; the light blue line and the shaded area represent, respectively, the ensemble mean of all possible solutions and ~~its variation~~ their range according to the ~~90~~95% CI.

Behavioral solutions obtained with PLTV revealed a similar pattern regardless of the interpolation employed (Fig. 4b, e, h and k). Nonetheless, there was a noticeable difference in the ~~90% CI~~ 95% CI of TT_{50} under distinct flow regimes. During low flows and dry periods (i.e., ~~late~~ summer and autumn), the time series of predicted TT_{50} ~~show~~ showed large uncertainties ranging at most between ~~286 and 895 days for the same moment in time~~ 259 and 1009 days across the different setups (Fig. 4e). Conversely, during high flows (i.e., winter and spring), the ~~90~~95% CI was ~~narrow~~ much narrower and varied at least between ~~135 and 163 days only~~ 129 and 160 days (Fig. 4h). The large ~~90~~95% CI and the notable differences across the tested setups highlight the sensitivity and, in turn, the uncertainty of predicted TT_{50} to the model parameterization, temporal interpolation of input data and hydrologic conditions. In contrast, the use of raw or kriged $\delta^{18}O_P$ samples produced ~~small differences~~ smaller differences as the trend in the estimated TT_{50} ~~; thus~~ was very similar. Thus, the spatial interpolation technique ~~did not substantially affect~~ impact less the water age simulations. However, the 95% CI of TT_{50} was larger when using raw rather than kriged $\delta^{18}O_P$ values.

In general, the variability of the predicted TT_{50} ~~is~~ was controlled by the hydrological state of the system (Fig. 4). ~~Discharge events reduced~~ High discharge events reduced the TT_{50} values, while low flow periods were associated with a longer estimated TT_{50}. This is expected as streamflow during high (low) flows is dominated by near-surface runoff (groundwater) with shallow (deep) flowpaths leading to a shorter (longer) TT_{50}. Such differences ~~are~~ were particularly visible with PLTV (Fig. 4b, e, h , and k) as the exponent $k_Q(t)$ ~~shifts~~ shift the water selection preference over time as a function of the wet/dry conditions~~; this makes~~

. This resulted in the variability of TT_{50} being more pronounced than that of PLTI and ~~BETA~~BETATI, whose SAS parameters for Q are constant over time.

4.3 ~~Use of the young water fraction (F_{yw})~~

~~The sine-wave fit produced young water fraction (F_{yw}^{est}) values equal to 0.25±0.08 and 0.22±0.07 for kriged and raw $\delta^{18}O_P$ samples, respectively. This means that approximately a quarter of the total streamflow is composed of water with ages younger than 2-3 months. Behavioral solutions produced SAS-based F_{yw}^{sim} values ranging between 0.22 and 0.54, across all tested setups, hence being much larger than F_{yw}^{est}. There were considerable differences in F_{yw}^{sim} across the SAS parameterizations as BETA produced a 37% larger F_{yw}^{sim} than that obtained with PLTI and PLTV, across the interpolation schemes. Moreover, F_{yw}^{sim} obtained with the sine interpolation was 31% larger than that of the step interpolation, across the tested setups. Conversely, no difference was found when using kriged or raw $\delta^{18}O_P$ samples.~~

~~**??** displays the simulated TT_{50} before (blue) and after (pink) using F_{yw}^{est} to reduce the uncertainty in the simulated TT_{50}. The results show that the addition of F_{yw}^{est} resulted in substantial changes in the 90% CI of TT_{50}, and the uncertainty reduction, in terms of percentage change, varied between 0% (Fig. **??**b, d and e) and 49% (Fig. **??**i) across the analysed setups. The lowest reduction occurred with the power law SAS functions and step function interpolation, with an average of 1% across the tested setups (Fig. **??**a, b, d and e). In contrast, the 90% CI was largely reduced with BETA and the sine interpolation with an average of 42% across the setups (Fig. **??**c, f, i and l). This clearly demonstrates the value of F_{yw}^{est} as an additional constraint in TT_{50} modelling.~~

~~Predicted TT_{50} for streamflow identified by 5% best KGE (blue) and by adding F_{yw}^{est} (pink); the light blue (pink) line and the shaded area represent, respectively, the ensemble mean of all possible solutions and its variation range according to the 90% CI.~~

4.3 Catchment-scale water release

SAS functions provided valuable insights into the catchment-scale water release dynamics. Figure 5 presents the behavioral solutions releasing water of different ages~~identified by 5% best KGE (blue) and after adding F_{yw}^{est} (pink), respectively. When considering the solutions identified by 5% best KGE, the~~ , and shows that the catchment generally experienced a stronger affinity for realising young water (i.e., k_Q<1, or α<1 and β>1), rather than old water (i.e., k_Q>1, or α>1 and β<1). These findings are in agreement with other studies in the Upper Selke (Winter et al., 2020; Nguyen et al., 2021). Nonetheless, ~~when PLTV is employed there is a considerable~~ there were differences in the water release scheme when comparing various combinations of SAS functions and spatio-temporal interpolation techniques of isotopes. The use of PLTV resulted in a substantial number of solutions~~indicating~~ , approximately 50% of all behavioral solutions, suggesting a preference for both young and old water. ~~Only~~ On the other hand, only a few solutions showed affinity for old water release, and this was ~~137%~~ more prominent when using the sine interpolation ~~and BETA,~~ technique, raw $\delta^{18}O_P$ values and PLTI across all tested setups.

~~The use of F_{yw}^{est} as additional constraint drastically changed the water release scheme for some of the tested setups. Figure 5 shows that the catchment mainly released old water when using the sine interpolation (Fig. 5g and h), especially with PLTV~~

and BETA. Although F_{yw}^{est} helped limit the uncertainty in the simulated TT_{50} under specific model assumptions, F_{yw}^{est} yielded contrasting results in the water release scheme, thus highlighting further sources of uncertainty related to those same setups.

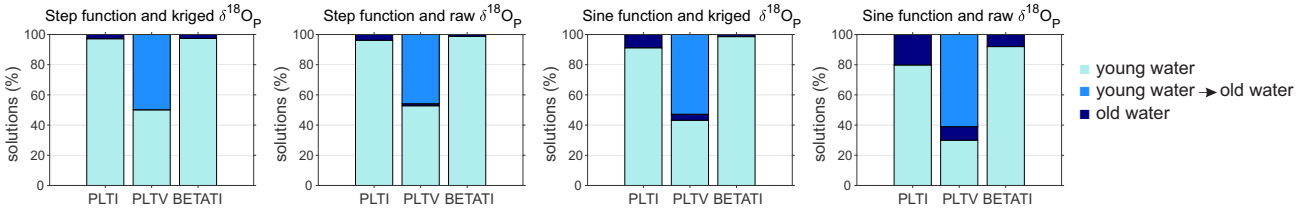

Figure 5. Percentage of behavioral solutions releasing water of different ages identified by 5% best KGE (blue) and by adding F_{yw}^{est} (pink).

5 Discussion

5.1 Uncertainty in TTD modelling

In this study, we characterized the TTD uncertainty arising from model inputs (i. e., tracer data interpolated in time and space) and structure (i. e., SAS parameterizations) some significant and critical aspects for the SAS modelling. These aspects are also the most directly linked to data interpolation and SAS parameterization that we explored in this work. The uncertainty analysis has been carried out across the twelve tested setups corresponding to different combinations of spatio-temporal data interpolation techniques and SAS parameterizations. Our results show that the uncertainty (i.e., 9095% CI) of the simulated TT_{50} (Fig. 4) was firmly dependent on the choice for the of model setup, and we found that the 90% CI was 95% CI is primarily sensitive to the SAS parameterizations as well as temporal interpolation of $\delta^{18}O_P$, rather than and less on the spatial interpolation of $\delta^{18}O_P$.

Uncertainty in the simulated TT_{50} differed considerably between time-invariant (i.e. PLTI and BETABETATI; Fig. 4a, c, d, f, g, i, j and l) and time-variant (i.e., PLTV; Fig. 4b, e, h and k) SAS functions. PLTI and BETA , thus a large sensitivity is associated with the choice of the SAS parameterization. For example, PLTI and BETATI explicitly assume constant water selection preference over time , creating as these functions do not consider temporal variability of the catchment wetness. As a consequence, the resulting simulations had a moderately stable 90% CI with small fluctuations . Moreover, for these SAS functions, the 90% CI is biased towards the long-term average discharge behavior, which might prevent a correct representation of the full TT_{50} variability during precipitation events and droughts (Buzacott et al., 2020). However, PLTI and BETA 95% CI in TT_{50} with smaller fluctuations compared to those of PLTV. Hence, the model setup with PLTI and BETATI could be appropriate where the catchment release scheme is expected to be relatively constantin catchments experiencing a less pronounced seasonality in streamflow and precipitation.

On the other hand, including an explicit time dependence in the SAS function strongly affected the 90% CI with respect to constant assumptions95% CI of TT_{50}. PLTV produced a wider 90% CI , 95% CI notably during low flow conditions, which can hinder the ability of the TTDs to provide robust insights on flow and solute transport behaviors in the study area during

low flow conditions. This highlights the need to further constrain PLTV with ~~further data~~additional data, which could involve obtaining tracer data at a finer resolution or additional information on the evapotranspiration and initial storage. In addition, the exceptionally old flow components associated with a very large ~~90% CI~~ 95% CI of TT_{50} might be a distortion of the actual TT_{50} ~~, as they are known to be better estimated with reactive~~ values, which can usually be more reliably estimated using radioactive tracers rather than stable isotopes (Visser et al., 2019). ~~Thus~~Hence, PLTV-based TT_{50} ~~that are~~ greater than the observed period (828 days) should be interpreted carefully.

~~Despite the sizeable 90% CI, PLTV could be more capable of capturing the hillslope activation and deactivation of flowpaths driven by the precipitation regime (Angermann et al., 2017; Loritz et al., 2017). Also, PLTV could infer information on the time-variant water selection preference that could not be derived with PLTI and BETA. Indeed, PLTV showed the inverse storageeffect, i.e., young water release during wet conditions rather than dry periods (Harman, 2015). This behavior may be the result of a rapid lateral transport due to rising water table (Pangle et al., 2017), and has been observed in many catchments (Benettin et al., 2017; Rodriguez et al., 2018; Wilusz et al., 2017, 2020)~~However, in this study we discussed the fractional (fSAS) functions, while another form of the SAS functions, such as the rank SAS (rSAS) functions, may have different uncertainty characteristics. This is mainly due to the difference in how the storage is considered, because fSAS functions are expressed as function of the normalized age-ranked storage, which is equal to the cumulative residence time, while rSAS functions depend on the age-ranked storage, which is the volume of water in storage ranked from youngest to oldest (Harman, 2015).

Likewise, the high-frequency reconstruction of $\delta^{18}O_P$ estimates from monthly values via interpolation created further uncertainty ~~, as real data provide insights that are irreplaceable~~that would not arise when using real high-frequency data. The sine interpolation poorly reproduced ~~heavily~~ flashy rainfall events and only captured the average damped trend of the observed $\delta^{18}O_P$ samples (Fig. S2 in the Supplement). Hence, related results must be interpreted with caution as tracer data uncertainty may conceal ~~more pronounced transport processes~~ a more pronounced hydrological response (Dunn et al., 2008; Birkel et al., 2010; Hrachowitz et al., 2011). Contrarily, the step function interpolation preserved the maxima in the monthly observed $\delta^{18}O_P$ values, and reproduced their variation correctly. ~~However, these results~~ Nonetheless, the results obtained in this study are based on this particular isotope dataset~~;~~, while the sine interpolation may be ~~suitably~~ better applicable in other circumstances. Overall, the temporal interpolation of tracers resulted in largely differing reconstructed input data depending on whether the step function or sine interpolation were used (Fig. S2 in the Supplement). This explains why the simulated TT_{50} is different between the two interpolations or, in other words, why the uncertainty in TT_{50} is large.

On the contrary, the spatial interpolation method did not strongly affect the simulated TT_{50} as the trend in the time series was similar when using kriged (Fig. 4a-c and g-i) or raw (Fig. 4d-f and j-l) $\delta^{18}O_P$. This could be attributed to minor differences between kriged and raw isotopes (Figs. S1 and S2 in the Supplement). Nonetheless, there was a larger 95% CI of TT_{50} when using raw rather than kriged $\delta^{18}O_P$, and this was particularly visible when the step function interpolation was used (Fig. 4a-f). Therefore, the spatial interpolation of $\delta^{18}O$ in precipitation from different locations resulted in an apparent reduction of uncertainty in TT_{50}.

In addition, we found that the uncertainty was larger under dry conditions when lower flow and longer TT_{50} were observed. This was especially visible when using the time-variant SAS function (Fig. 4b, e, h and k). It might be due to the fact that under wet conditions, there is a high level of hydrologic connectivity within the catchment (Ambroise, 2004; Blume and van Meerveld, 2015; Hrachowitz et al., 2016), which results in nearly all flow paths being active and contributing to the streamflow that, ultimately, may make TT_{50} values easier to constrain. Conversely, under dry conditions, when there is low connectivity within the catchment, only certain flow paths are active, i.e., usually those carrying older water to the stream (Soulsby and Tetzlaff, 2008; Jasechko et al., 2017). Hence, these flows are less uniform, making it more challenging to constrain their older water ages. Similarly, Benettin et al. (2017) found higher uncertainty in the simulated SAS-based median water ages during drier periods, potentially due to higher uncertainty in the total storage. Moreover, non-SAS functions studies have observed major uncertainties and deviations from observations in lumped modeled results during low flow conditions (Kumar et al., 2010). This was primarily due to the lack of spatial variability of catchment characteristics in lumped models, a critical factor controlling low flow regimes in rivers.

The dissimilarities in the simulated TT_{50} across the tested setups underline the importance of accounting for uncertainty in model-based TTDs. The uncertainty analysis with SUFI-2 performed in this study was essential to best describe the parameter identifiability and bounds of the behavioral solutions of each output variable. Furthermore, our results highlight the importance of gaining ~~a good qualityfor tracer datatasets~~ tracer datasets of good quality, meaning tracer data with a finer resolution, and, possibly, employing the ~~"true"~~ "true" model parameterization which correctly describes the ~~catchment area~~catchment-specific storage and release dynamics. The second point can be defined according to a precise conceptual knowledge of the catchment's functioning ~~(e.g., the geometry of the flow system)~~ and information from previous studies in similar catchments.

5.2 ~~On the value of young water fraction~~

~~The use of F_{yw}^{est} succeeded in limiting the uncertainty in the predicted TT_{50} obtained from the sine interpolation of $\delta^{18}O_P$ values and BETA. This reveals how these two setups combined are characterized by a high degree of uncertainty which is propagated into the simulated TT_{50}. We acknowledge that this is due to the sine interpolation, which only captured the average depleted trend of $\delta^{18}O_P$ values (Fig. S2 in the Supplement). In addition, BETA is characterized by numerous behavioral solutions skewed towards short TT_{50} values and, in turn, large F_{yw}^{sim} (Fig. 4i and l), which might not correctly represent the TT_{50} values in the study area.~~

~~We recognize the robustness of F_{yw}^{est} obtained by the sine regression to ensure reliable TT_{50} values in this study. We attribute this to the moderately small standard errors in F_{yw}^{est} (0.07 and 0.08 for raw and kriged $\delta^{18}O_P$ values, respectively). This is partly due to the fact that we used the same sampling period for $\delta^{18}O$ in precipitation and streamflow, which limits the uncertainty of estimated F_{yw}^{est}.~~

~~A higher temporal resolution of isotope samples rather than a coarser one could prevent bias toward smaller F_{yw}^{est} (Stockinger et al., 2016; Lutz et al., 2018), Also, to better represent the estimated F_{yw}^{est} from the sine regression, we could incorporate processes affecting the isotopic composition such as snowmelt (von Freyberg et al., 2018; Ceperley et al., 2020).~~

~~Despite these limitations, based on our analysis, we acknowledge the potential of using F_{yw}^{est} for improving TTD predictions and limiting their uncertainty.~~

5.2 TTD modelling: advantages and limitations

Our results provide visually plausible seasonal fluctuations of the predicted $\delta^{18}O_Q$ samples (Fig. 2), and satisfactory KGE values (Fig. 3), despite the uncertainty arising from ~~both model inputsand structure . This corroborates our findings for~~ model inputs, structure and parameters. The good match with observations provides high confidence in the simulated TT_{50} ~~in~~ for the Upper Selke. The magnitude of the uncertainty resulting from different setups cannot be generalized, but the overall approach for uncertainty assessment presented here could be extended to other areas and TTD studies. However, we recognize some limitations and ~~below indicate~~ indicate below possible reasons and, in turn, improvements that future work could achieve.

First, the limited length of the $\delta^{18}O$ ~~timeseries~~ time series might not describe the system accurately~~. Implementing longer timeseries~~, hence implementing longer time series could improve the parameter identifiability and provide a ~~closer approximation~~ more accurate estimation of the TTDs. Second, this study relied ~~only~~ on stable water isotopes, which might underestimate the tails of the TTDs ~~(Stewart et al., 2010; Seeger and Weiler, 2014)~~ (Stewart et al., 2010; Seeger and Weiler, 2014; Wang et al., 2022). Possible advancements could be reached by using decaying tracers varying over a larger timescale than stable water isotopes (e.g., tritium, (Stewart et al., 2012; Morgenstern et al., 2015)), and imparting more information on old water. Next, future work should retrieve more information on *ET* and the initial storage S_0, whose parameters were poorly identified. However, this issue is common in transport studies that rely on measurements of instream stable water ~~isotope~~ isotopes (Benettin et al., 2017; Buzacott et al., 2020). As a way forward, information on the *ET* isotopic compositions might help better constrain *ET* ~~*ET*~~ parameters and assess their affinity for young/old water. Regarding constraining the range of S_0, further information can be gained ~~knowing the geophysical properties of catchment (i.e., geological structure and physical characteristics) (Holbrook et al., 2014), and~~ from geophysical surveys in the study areas or groundwater modeling, as well as using decaying isotopes (Visser et al., 2019). ~~Finally, future research should better explore the validity of F_{yw} to limit the predictive uncertainty in TTDs, by exploring whether the effectiveness of F_{yw} for TTD estimation depends on catchment's attributes (e.g., size, annual precipitation, flow rates, soil and vegetation).~~

5.3 Implications of TTD uncertainties

This study characterized the uncertainty in TTDs, which summarize the catchment's hydrologic transport behavior, and thereby comprise decisive information for water managers. The uncertainty in the predicted TT_{50} has relevant implications for both water quantity and quality; the larger the ~~90~~95% CI in the simulated TT_{50}, the greater the difference in the TT_{50} values, which, ultimately, implies distinct water release and solute export dynamics (McDonnel et al., 2010).

Uncertainty in TTDs may be crucial for characterizing the catchment's response to climatic changes (Wilusz et al., 2017). Considering the increasing severity of droughts in the past decades (Dai, 2013), a catchment that largely releases young water might be more affected by droughts than a catchment whose stream is fed by relatively old water sources. A short TT_{50} reveals a low drought resilience of the catchment, which could limit streamflow generation processes and change the instream water

quality status. Likewise, TTD uncertainty may affect the quantification of ~~te~~ the modern groundwater age, i.e., groundwater younger than 50 years (Bethke and Johnson, 2008). According to (Jasecko, 2019), the correct identification of modern groundwater abundance and distribution can help determine its renewal (Le Gal La Salle et al., 2001; Huang et al., 2017), groundwater wells and depths most likely to contain contaminants (Visser et al., 2013; Opazo et al., 2016), and the part of the aquifer flushed more rapidly.

Uncertainty in TTDs also impacts on assessing the fate of dissolved solutes, such as nitrates ~~(Yang, X. et al., 2018; Nguyen et al., 2021)~~(Yang, X. et al., 2018; Nguyen et al., 2021, 2022), pesticides (Holvoet et al., 2007; Lutz et al., 2017), and chlorides (Kirchner et al., 2000; Benettin et al., 2013). These solutes constitute a crucial source of diffuse water pollution in agricultural areas (Jiang et al., 2014; Kumar et al., 2020), as they are spread on the soil ~~during the fertilization period~~in large quantities especially during the growing season. Exposure time of ~~nitrates~~ solutes with the soil matrix has strong consequences for biogeochemical reactions, such as denitrification in the case of nitrates (Kolbe et al., 2019; Kumar et al., 2020). A short TT_{50} suggests that water can be rapidly conveyed to the stream network (Kirchner et al., 2001), with limited time for denitrification. This explains the elevated instream concentration and short-term impact of nitrate export compared to that of a longer TT_{50}, which is typically associated with old water release and low nitrate concentration (Nguyen et al., 2021). Similarly, pesticide transport is highly affected by the TTD uncertainty as a long TT_{50} ~~may decelerate~~ suggests little pesticide degradation due to decreased microbial activity along deeper flowpaths (Rodríguez-Cruz et al., 2006). In other cases, a shorter TT_{50} may ~~limits~~ limit the time for degradation causing a peak in the instream concentration (Leu et al., 2004). Overall, a longer TT_{50} can delay or buffer the catchment's reactive solute response at the outlet (Dupas et al., 2016; Van Meter et al., 2017). This creates a long-term effect of hydrological legacies and a continuous problem with diffuse pollution of nitrates (Ehrhardt et al., 2019; Winter et al., 2020) and pesticides (Lutz et al., 2013), which can persist in the catchment for several years. Finally, TTD uncertainties also play an important role in chloride transport, although chlorides are commonly known to be conservative (Svensson et al., 2012). A short TT_{50} may indicate rapid chloride mobilization, whereas a long TT_{50} implies chloride persistence in groundwater; thereby chloride accumulates and is released at lower rates, with impacts on the ecosystem functions, vegetation uptake and metabolism (Xu et al., 1999).

Understanding the uncertainty in TTDs is crucial for the aforementioned implications. ~~In this study, we want to convey that it is essential to characterize the specific sources of uncertainty, which can stem from model inputs, structure and parameters, as well as their combined effects on the predicted TTDs. Uncertainty~~ While previous studies have used only a specific SAS function and/or specific data fitting technique, here we show that there could be a wide range of different results in terms of water ages, model performances and parameter uncertainty. This is due to the specific choice regarding SAS parameterization and tracer data interpolation. With this, we want to convey that uncertainty is omnipresent in TTD-based ~~modeling~~models, and we need to recognise it, especially when dealing with sparse tracer data and multiple choices for model parameterization~~, which affect the calculated TT_{50}. We also acknowledge the potential of incorporating additional information on water ages based on F_{yw}, which has contributed to reduce TT_{50} uncertainties~~. Therefore, we want to encourage future studies to explore these uncertainties in other catchments and different geophysical settings, with the final aim to investigate whether these uncertainties may affect the conclusions of water quantity and quality studies for management purposes.

6 Conclusions

This study explored the uncertainty in TTDs of streamflow, resulting from twelve model setups obtained from different SAS parameterizations (i.e., PLTI, PLTV and ~~BETA~~BETATI), and reconstruction of the precipitation isotopic signature in time and space via interpolation (step function vs. sine-fit, raw vs. kriged values).

We found satisfactory KGE values, whose differences across the tested setups were statistically significant, meaning that the choice of the setup matters~~and, as~~ . As a consequence, distinct setups led to considerably different simulated TT_{50} values. The choice between using time-variant or time-invariant SAS functions was crucial as the time-invariant ~~SAS function generated a bias in~~ functions generated a moderately stable 95% CI of the estimated TT_{50} ~~toward the long-term average discharge behavior, which might be appropriate for catchments experiencing smooth changes in the hydrologic conditions.~~ because of the constant water selection preference over time. These functions may be more appropriate for those catchments experiencing relatively little seasonality in the hydrological conditions.

On the other hand, the time-variant SAS function captured the dynamics of the catchment wetness, resulting in ~~very high~~ a pronounced seasonality of TT_{50}. However, the time-variant SAS function also produced a larger ~~90% CI , which indicates~~ 95% CI in TT_{50}, notably during drier periods, which might indicate the need to constrain the function with additional data ~~.~~ (e.g., finer tracer data resolution, and/or information on evapotranspiration and storage). Significant differences in TT_{50} were observed depending on the employed temporal interpolations. Results from the ~~temporal interpolation using a sine curve~~ sine interpolation must be interpreted carefully as they poorly reproduced flashy events in precipitation, thus indicating that some more dynamic transport processes were not fully accounted for. Conversely, the step function interpolation was able to ~~intercept~~ better reproduce the measured $\delta^{18}O_P$ data. Dry conditions were another reason for uncertainty as indicated by the high variance in the simulated TT_{50} values. Finally, the use of ~~F_{yw} as an additional constraint was promising in reducing TT_{50} uncertainties, particularly when using the sine interpolation of~~ spatial interpolation methods did not substantially affect the uncertainty in TT_{50} as there were no appreciable differences in the trend of the modeled results between kriged and raw isotopes, although the 95% CI in TT_{50} was wider when using raw $\delta^{18}O_P$~~samples combined with BETA~~.

Our study provides new insights into ~~the TTDs~~ TTD uncertainty when high-frequency tracer data are missing and the SAS framework is used. Regardless of the degree of efficiency or uncertainty, the decision on which setup is more plausible depends on a full conceptual knowledge of the catchment functioning. We consider the presented approach as potentially applicable to other studies for enabling a better characterization of TTDs uncertainty, improving TTD simulations and, ultimately, informing water management. These aspects are particularly crucial in view of evermore extreme climatic conditions and increasing water pollution under global change.

Code and data availability. The model used in this study is presented at https://doi.org/10.5194/gmd-11-1627-2018. The iteratively re-weighted least squares (IRLS) method used to get modelled daily kriged and raw isotope ($\delta^{18}O$) in precipitation with the sine interpolation is presented at https://doi.org/10.5194/hess-22-3841-2018. Hydrocliamtic time series, $\delta^{18}O$ data and interpolated $\delta^{18}O$ time series can be accessed at https://doi.org/10.5281/zenodo.6630477.

Author contributions. AB conducted the model simulations, the analysis and interpretation of the results, and wrote the original draft of the paper. SRL and RK designed and conceptualized the study, and provided data for model simulations. TVN provided technical support for modelling and helped organize the structure and content of the paper. AB, SRL, RK and TVN conceived the methodology and experimental design. All co-authors helped AB interpret the results. All authors contributed to the review, final writing and finalization of this work.

Competing interests. RK is a member of the editorial board of Hydrology and Earth System Sciences.

References

Abbaspour, K. C., Johnson, C. A., and van Genuchten, M. T.: Estimating uncertain flow and transport parameters using a sequential uncertainty fitting procedure, Vadose Zone Journal, 3(4), 1340–1352, https://doi.org/10.2136/vzj2004.1340, 2004.

Ajami, N. K., Duan, Q., and Sorooshian, S.: An integrated hydrologic Bayesian multimodel combination framework: Confronting input, parameter, and model structural uncertainty in hydrologic prediction, Water Resour. Res., 43, W01 403, https://doi.org/10.1029/2005WR004745, 2007.

Ambroise, B.: Variable 'active' versus 'contributing' areas or periods: a necessary distinction, Hydrol. Process., 18, 1149–1155, https://doi.org/10.1002/hyp.5536, 2004.

Andersson, J. C. M., Arheimer, B., Traoré, F., Gustafsson, D., , and Ali, A.: Process refinements improve a hydrological model concept applied to the Niger River basin, Hydrol. Process., 31, 4540–4554, https://doi.org/10.1002/hyp.11376, 2017.

Angermann, L., Jackisch, C., Allroggen, N., Sprenger, M., Zehe, E., Tronicke, J., Wiler, M., and Blume, T.: Form and function in hillslope hydrology: characterization of subsurface flow based on response observations, Hydrol. Earth Syst. Sci., 21, 3727–3748, https://doi.org/10.5194/hess-21-3727-2017, 2017.

Asadollahi, M., Stumpp, C., Rinaldo, A., and Benettin, P.: Transport and water age dynamics in soils: A comparative study of spatially integrated and spatially explicit models, Water Resour. Res., 56, e2019WR025 539, https://doi.org/10.1029/2019WR025539, 2020.

Benettin, P. and Bertuzzo, E.: tran-SAS v1.0: a numerical model to compute catchment-scale hydrologic transport using StorAge Selection functions, Geosci. Model Dev., 11, 1627–1639, https://doi.org/10.5194/gmd-11-1627-2018, 2018.

Benettin, P., van der Velde, Y., van der Zee, S. E. A. T. M., Rinaldo, A., and Botter, G.: Chloride circulation in a lowland catchment and the formulation of transport by travel time distributions, Water Resour. Res., 49, 4619–4632, https://doi.org/10.1002/wrcr.20309, 2013.

Benettin, P., Bailey, S. W., Campbell, J. L., Green, M. B., Rinaldo, A., Likens, G. E., J., M. K., and Botter, G.: Linking water age and solute dynamics in streamflow at the Hubbard Brook Experimental Forest, NH, USA, Water Resour. Res., 51, 9256–9272, https://doi.org/10.1002/2015WR017552, 2015a.

Benettin, P., Kirchner, J. W., Rinaldo, A., and Botter, G.: Modeling chloride transport using travel time distributions at Plynlimon, Wales, Water Resour. Res., 51, 3259–3276, https://doi.org/10.1002/2014WR016600, 2015b.

Benettin, P., Soulsby, C., Birkel, C., Tetzlaff, D., Botter, G., and Rinaldo, A.: Using SAS functions and high-resolution isotope data to unravel travel time distributions in headwater catchments, Water Resour. Res., 53, 1864–1878, https://doi.org/10.1002/2016WR020117, 2017.

Bethke, C. M. and Johnson, T. M.: Groundwater age and groundwater age dating, Annu. Rev. Earth Planet. Sci., 36, 121–152, https://doi.org/10.1146/annurev.earth.36.031207.124210, 2008.

Beven, K.: A manifesto for the equifinality thesis, J. Hydrol., 320, 18–36, https://doi.org/10.1016/j.jhydrol.2005.07.007, 2006.

Beven, K. and Binley, A.: The future of distributed models: model calibration and uncertainty prediction, Hydrol. Process., 6, 279–298, https://doi.org/10.1002/hyp.3360060305, 1992.

Beven, K. and Freer, J.: Equifinality, data assimilation, and uncertainty estimation in mechanistic modelling of complex environmental systems using the GLUE methodology, J. Hydrol., 249, 11–29, https://doi.org/10.1016/S0022-1694(01)00421-8, 2001.

Birkel, C. and Soulsby, C.: Advancing tracer-aided rainfall-runoff modelling: A review of progress, problems and unrealised potential, Hydrol. Process., 29, 5227–5240, https://doi.org/10.1002/hyp.10594, 2015.

Birkel, C., Dunn, S. M., Tetzlaff, D., and Soulsby, C.: Assessing the value of high-resolution isotope tracer data in the stepwise development of a lumped conceptual rainfall–runoff model, Hydrol. Process., 24, 2335–2348, https://doi.org/10.1002/hyp.7763, 2010.

Bliss, C. I.: Statistics in biology: Statistical methods for research in the natural sciences (Vol. 2), New York: McGraw-Hill, https://doi.org/10.1002/bimj.19690110327, 1970.

Blume, T. and van Meerveld, H. J.: From hillslope to stream: methods to investigate subsurface connectivity, WIREs Water, 2, 177–198, https://doi.org/10.1002/wat2.1071, 2015.

Botter, G., Bertuzzo, E., Bellin, A., and Rinaldo, A.: On the Lagrangian formulations of reactive solute transport in the hydrologic response, Water Resour. Res., 41, W04 008, https://doi.org/10.1029/2004WR003544, 2005.

Botter, G., Bertuzzo, E., and Rinaldo, A.: Transport in the hydrologic response: Travel time distributions, soil moisture dynamics, and the old water paradox, Water Resour. Res., 46, W03 514, https://doi.org/10.1029/2009WR008371, 2010.

Botter, G., Bertuzzo, E., and Rinaldo, A.: Catchment residence and travel time distributions: The master equation, Geophys. Res. Lett., 38, L11 403, https://doi.org/10.1029/2011GL047666, 2011.

Buzacott, A. J. V., van der Velde, Y., Keitel, C., and Vervoort, R. W.: Constraining water age dynamics in a south-eastern Australian catchment using an age-ranked storage and stable isotope approach, Hydrol. Process., 34, 4384–4403, https://doi.org/10.1002/hyp.13880, 2020.

Ceperley, N. Zuecco, G., Beria, H., Carturan, L., Michelon, A., Penna, D., Larsen, J., and Schaefli, B.: Seasonal snow cover decreases young water fractions in high Alpine catchments, Hydrol. Process., 34, 4794–4813, https://doi.org/10.1002/hyp.13937, 2020.

Dai, A.: Erratum: Increasing drought under global warming in observations and models, Nature Clim Change, 3, 171, https://doi.org/10.1038/nclimate1811, 2013.

Danesh-Yazdi, M., Foufoula-Georgiou, E., Karwan, D. L., and Botter, G.: Inferring changes in water cycle dynamics of intensively managed landscapes via the theory of time-variant travel time distributions, Water Resour. Res., 52, 7593–7614, https://doi.org/10.1002/2016WR019091, 2016.

Danesh-Yazdi, M., Klaus, J., Condon, L. E., and Maxwell, R. M.: Bridging the gap between numerical solutions of travel time distributions and analytical storage selection functions, Hydrol. Process., 32, 1063–1076, https://doi.org/10.1002/hyp.11481, 2018.

Yang, J., Heidbüchel, I., Musolff, A., Reinstorf, F., and Fleckenstein, J. H.: Exploring the Dynamics of Transit Times and Subsurface Mixing in a Small Agricultural Catchment, Water Resour. Res., 54, 2317–2335, https://doi.org/10.1002/2017WR021896, 2018.

Yang, X., Seifeddine, J., Zink, M., Fleckenstein, J. H., Borchardt, D., and Rode, M.: A New Fully Distributed Model of Nitrate Transport and Removal at Catchment Scale, Water Resour. Res., 54, 5856–5877, https://doi.org/10.1029/2017WR022380, 2018.

Drever, M. C. and Hrachowitz, M.: Migration as flow: using hydrological concepts to estimate the residence time of migrating birds from the daily counts, Methods Ecol. Evol., 8, 1146–1157, https://doi.org/10.1111/2041-210X.12727, 2017.

Dunn, S. M., Bacon, J. R., Soulsby, C., Tetzlaff, D., Stutter, M. I., Waldron, S., and Malcolm, I. A.: Interpretation of homogeneity in δ^{18}O signatures of stream water in a nested sub-catchment system in north-east Scotland, Hydrol. Process., 22, 4767–4782, https://doi.org/10.1002/hyp.7088, 2008.

Dupas, R., Jomaa, S., Musolff, A., Borchardt, D., and Rode, M.: Disentangling the influence of hydroclimatic patterns and agricultural management on river nitrate dynamics from sub-hourly to decadal time scales, Sci. Total Environ., 571, 791–800, https://doi.org/10.1016/j.scitotenv.2016.07.053, 2016.

Dupas, R., Musolff, A., Jawitz, J. W., Rao, P. S. C., Jäger, C. G., Fleckenstein, J. H., Rode, M., and Borchardt, D.: Carbon and nutrient export regimes from headwater catchments to downstream reaches, Biogeosciences, 14, 4391–4407, https://doi.org/10.5194/bg-14-4391-2017, 2017.

Duvert, C., Stewart, M. K., Cendon, D. I., and Raiber, M.: Time series of tritium, stable isotopes and chloride reveal short-term variations in groundwater contribution to a stream, Hydrol. Earth Syst. Sci.,, 20, 257–277, https://doi.org/10.5194/hess-20-257-2016, 2016.

Ehrhardt, S., Kumar, R., Fleckenstein, J. H., Attinger, S., and Musolff, A.: Trajectories of nitrate input and output in three nested catchments along a land use gradient, Hydrol. Earth Syst. Sci., 23, 3503–3524, https://doi.org/10.5194/hess-23-3503-2019, 2019.

Feng, X., Faiia, A. M., and Posmentier, E. S.: Seasonality of isotopes in precipitation: A global perspective, J. Geophys. Res, 114, D08 116, https://doi.org/10.1029/2008jd011279, 2009.

Gupta, H. V., Kling, H., Yilmaz, K. K., and Martinez, G. F.: Decomposition of the mean squared error and NSE performance criteria: Implications for improving hydrological modelling, J. Hydrol., 377, 80–91, https://doi.org/10.1016/j.jhydrol.2009.08.003, 2009.

Harman, C. J.: Time-variable transit time distributions and transport: Theory and application to storage-dependent transport of chloride in a watershed, Water Resour. Res., 51, 1–30, https://doi.org/10.1002/2014WR015707, 2015.

Harman, C. J.: Age-Ranked Storage-Discharge Relations: A Unified Description of Spatially Lumped Flow and Water Age in Hydrologic Systems, Water Resour. Res., 55, 7143–7165, https://doi.org/10.1029/2017WR022304, 2019.

Heidbüchel, I., Yang, J., Musolff, A., Troch, P., Ferré, T., and Fleckenstein, J. H.: On the shape of forward transit time distributions in low-order catchments, Hydrol. Earth Syst. Sci., 24, 2895–2920, https://doi.org/10.5194/hess-24-2895-2020, 2020.

Heidbüchel, I., Troch, P. A., Lyon, S. W., and Wiler, M.: The master transit time distribution of variable flow systems, Water Resour. Res., 48, W06 520, https://doi.org/10.1029/2011WR011293, 2012.

Heidbüchel, I., Troch, P. A., and Lyon, S. W.: Separating physical and meteorological controls of variable transit times in zero-order catchments, Water Resour. Res., 49, 7644—-7657, https://doi.org/10.1002/2012WR013149, 2013.

Holbrook, W. S., Riebe, C. S., Elwaseif, M., Hayes, J. L., Basler-Reeder, K., Harry, D. L., Malazian, A., Dosseto, A., Hartsough, P. C., and Hopmans, J. W.: Geophysical constraints on deep weathering and water storage potential in the Southern Sierra Critical Zone Observatory, Earth Surface Processes and Landforms, 39, 366–380, https://doi.org/10.1002/esp.3502, 2014.

Holvoet, K. M., Seuntjens, P., and Vanrolleghem, P. A.: Monitoring and modeling pesticide fate in surface waters at the catchment scale, Ecol. Model., 209, 53–64, https://doi.org/10.1016/j.ecolmodel.2007.07.030, 2007.

Hrachowitz, M., Soulsby, C., Tetzlaff, D., Malcolm, I. A., and Schoups, G.: Gamma distribution models for transit time estimation in catchments: Physical interpretation of parameters and implications for time-variant transit time assessment, Water Resour. Res., 46, W10 536, https://doi.org/10.1029/2010WR009148, 2010.

Hrachowitz, M., Soulsby, C., Tetzlaff, D., and Malcolm, I. A.: Sensitivity of mean transit time estimates to model conditioning and data availability, Hydrol. Process., 25, 980–990, https://doi.org/10.1002/hyp.7922, 2011.

Hrachowitz, M., Savenije, H., Bogaard, T. A., Tetzlaff, D., and Soulsby, C.: What can flux tracking teach us about water age distribution patterns and their temporal dynamics?, Hydrol. Earth Syst. Sci, 17, 533–564, https://doi.org/10.5194/hess-17-533-2013, 2013.

Hrachowitz, M., Benettin, P., van Breukelen, B. M., Fovet, O., Howden, N. J. K., Ruiz, L van der Velde, Y., and Wade, A. J.: Transit times — the link between hydrology and water quality at the catchment scale, WIREs Water, 3, 629–657, https://doi.org/10.1002/wat2.1155, 2016.

Huang, T., Pang, Z., Li, J., Xiang, Y., and Zhao, Z.: Mapping groundwater renewability using age data in the Baiyang alluvial fan, NW, China, Hydrogeol J., 25, 743–755, https://doi.org/10.1007/s10040-017-1534-z, 2017.

Jasechko, S., Wassenaar, L. I., and Mayer, B.: Isotopic evidence for widespread cold-season-biased groundwater recharge and young streamflow across central Canada, Hydrol. Process., 31, 2196–2209, https://doi.org/10.1002/hyp.11175, 2017.

Jasecko, S.: Global isotope hydrogeology — review, Reviews of Geophysics, 57, 835–965, https://doi.org/10.1029/2018RG000627, 2019.

Jiang, S., Jomaa, S., and Rode, M.: Modelling inorganic nitrogen leaching in nested mesoscale catchments in central Germany, Ecohydrol., 7, 1345–1362, https://doi.org/10.1002/eco.1462, 2014.

Jing, M., Heße, F., Kumar, R., Kolditz, O., Kalbacher, T., and Attinger, S.: Influence of input and parameter uncertainty on the prediction of catchment-scale groundwater travel time distributions, Hydrol. Earth Syst. Sci., 23, 171–190, https://doi.org/10.5194/hess-23-171-2019, 2019.

Kim, M. and Troch, P. A.: Transit time distributions estimation exploiting flow-weighted time: Theory and proof-of-concept, Water Resour. Res., 56, e2020WR027 186, https://doi.org/10.1029/2020WR027186, 2022.

Kim, M., Pangle, L. A., Cardoso, C., Lora, M., Volkmann, T. H. M., Wang, Y., Harman, C. J., and Troch, P. A.: Transit time distributions and StorAge Selection functions in a sloping soil lysimeter with time-varying flow paths: Direct observation of internal and external transport variability, Water Resour. Res., 52, 7105–7129, https://doi.org/10.1002/2016WR018620, 2016.

Kirchner, J. W.: Getting the right answers for the right reasons: Linking measurements, analyses, and models to advance the science of hydrology, Water Resour. Res., 42, W03S04, https://doi.org/10.1029/2005WR004362, 2006.

Kirchner, J. W.: Aggregation in environmental systems – Part 1: Seasonal tracer cycles quantify young water fractions, but not mean transit times, in spatially heterogeneous catchments, Hydrol. Earth Syst. Sci., 20, 279–297, https://doi.org/10.5194/hess-20-279-2016, 2016a.

Kirchner, J. W.: Aggregation in environmental systems – Part 2: Catchment mean transit times and young water fractions under hydrologic nonstationarity, Hydrol. Earth Syst. Sci., 20, 299–328, https://doi.org/10.5194/hess-20-299-2016, 2016b.

Kirchner, J. W.: Quantifying new water fractions and transit time distributions using ensemble hydrograph separation: theory and benchmark tests, Hydrol. Earth Syst. Sci., 23, 303–349, https://doi.org/10.5194/hess-23-303-2019, 2019.

Kirchner, J. W., Feng, X., and Neal, C.: Fractal stream chemistry and its implications for contaminant transport in catchments, Nature, 403, 524–527, https://doi.org/10.1038/35000537, 2000.

Kirchner, J. W., Feng, X., and Neal, C.: Catchment-scale advection and dispersion as a mechanism for fractal scaling in stream tracer concentrations, J. Hydrol., 254, 82–101, https://doi.org/10.1016/S0022-1694(01)00487-5, 2001.

Kirchner, J. W., Feng, X., Neal, C., and Robson, A. J.: The fine structure of water-quality dynamics: the (high-frequency) wave of the future, Hydrol. Process., 18, 1353–1359, https://doi.org/10.1002/hyp.5537, 2004.

Kolbe, T., de Dreuzy, J. R., Abbott, B. W., Aquilina, L., Babey, T., Green, C. T., et al.: Stratification of reactivity determines nitrate removal in groundwater, Proceedings of the National Academy of Sciences, 116(7), 2494–2499, https://doi.org/10.1073/pnas.1816892116, 2019.

Kumar, R., Samaniego, L., and S., A.: The effects of spatial discretization and model parameterization on the prediction of extreme runoff characteristics, J. Hydrol., 392, 54–69, https://doi.org/10.1016/j.jhydrol.2010.07.047, 2010.

Kumar, R., Samaniego, L., and Attinger, S.: Implications of distributed hydrologic model parameterization on water fluxes at multiple scales and locations, Water Resour. Res., 49, 360–379, https://doi.org/10.1029/2012WR012195, 2013.

Kumar, R., Heße, F., Rao, P. S. C., Musolff, A., Jawitz, J. W., Sarrazin, F., Samaniego, L., Fleckenstein, J. H., Rakovec, O., Thober, S., and Attinger, S.: Strong hydroclimatic controls on vulnerability to subsurface nitrate contamination across Europe, Nature Communications, 11, 6302, https://doi.org/10.1038/s41467-020-19955-8, 2020.

Le Gal La Salle, C., Marlin, C., Leduc, C., Taupin, J. D., Massault, M., and Favreau, G.: Renewal rate estimation of groundwater based on radioactive tracers (3H, 14C) in an unconfined aquifer in a semi-arid area, Iullemeden Basin, Niger, J. Hydrol., 254, 145–156, https://doi.org/10.1016/S0022-1694(01)00491-7, 2001.

Leu, C., Singer, H., Stamm, C., Muller, S. R., and Schwarzenbach, R. P.: Simultaneous Assessment of Sources, Processes, and Factors Influencing Herbicide Losses to Surface Waters in a Small Agricultural Catchment, Environ. Sci. Technol., 38, 3827–3834, https://doi.org/10.1021/es0499602, 2004.

Loritz, R., Hassler, S. K., Jackisch, C., Allroggen, N., van Schaik, L., Wienhöfer, J., and Zehe, E.: Picturing and modeling catchments by representative hillslopes, Hydrol. Earth Syst. Sci., 21, 1225–1249, https://doi.org/10.5194/hess-21-1225-2017, 2017.

Lutz, S., van Meerveld, H. J., Waterloo, M. J., Broers, H. P., and van Breukelen B. M.: A model-based assessment of the potential use of compound-specific stable isotope analysis in river monitoring of diffuse pesticide pollution, Hydrol. Earth Syst. Sci., 17, 4505–4524, https://doi.org/10.5194/hess-17-4505-2013, 2013.

Lutz, S. R., van der Velde, Y., Elsayed, O. F., Imfeld, G., Lefrancq, M., Payraudeau, S., and van Breukelen, B. M.: Pesticide fate on catchment scale: conceptual modelling of stream CSIA data, Hydrol. Earth Syst. Sci., 21, 5243–5261, https://doi.org/10.5194/hess-21-5243-2017, 2017.

Lutz, S. R., Krieg, R., Müller, C., Zink, M., Knöller, K., Samaniego, L., and Merz, R.: Spatial patterns of water age: using young water fractions to improve the characterization of transit times in contrasting catchments, Water Resour. Res., 54, 4767–4784, https://doi.org/10.1029/2017WR022216, 2018.

McDonnel, J. J., McGuire, K., Aggarwal, P., Beven, K. J., Biondi, D., Destouni, G., et al.: How old is streamwater? Open questions in catchment transit time conceptualization, modelling and analysis, Hydrol. Process., 24, 1745–1754, https://doi.org/10.1002/hyp.7796, 2010.

McGuire, K. J. and McDonnel, J. J.: A review and evaluation of catchment transit time modeling, J. Hydrol., 330, 543–563, https://doi.org/10.1016/j.jhydrol.2006.04.020, 2006.

McKay, M. D., Beckman, R. J., and Conover, W. J.: A Comparison of Three Methods for Selecting Values of Input Variables in the Analysis of Output from a Computer Code, Technometrics, 21, 239–245, https://doi.org/10.2307/1268522, 1979.

Morgenstern, U., Daughney, C. J., Leonard, G., Gordon, D., Donath, F. M., and Reeves, R.: Using groundwater age and hydrochemistry to understand sources and dynamics of nutrient contamination through the catchment into Lake Rotorua, New Zealand, Hydrol. Earth Syst. Sci., 19, 803–822, https://doi.org/10.5194/hess-19-803-2015, 2015.

Nguyen, T. V., Kumar, R., Lutz, S. R., Musolff, A., Yang, J., and Fleckenstein, J. H.: Modeling Nitrate Export From a Mesoscale Catchment Using StorAge Selection Functions, Water Resour. Res., 57, e2020WR028 490, https://doi.org/10.1029/2020WR028490, 2021.

Nguyen, T. V., Sarrazin, F. J., Ebeling, P., Musolff, A., Fleckenstein, J. H., and Kumar, R.: Toward Understanding of Long-Term Nitrogen Transport and Retention Dynamics Across German Catchments, Geophysical Research Letters, 49, e2022GL100 278, 2022.

Niemi, A. J.: Residence time distributions of variable flow processes, The International Journal of Applied Radiation and Isotopes, 28(10), 855–860, https://doi.org/10.1016/0020-708X(77)90026-6, 1977.

Opazo, T., Aravena, R., and Parker, B.: Nitrate distribution and potential attenuation mechanisms of a municipal water supply bedrock aquifer, Applied Geochemistry, 73, 157–168, https://doi.org/10.1016/j.apgeochem.2016.08.010, 2016.

Pangle, L. A., Kim, M., Cardoso, C., Lora, M., Meira Neto, A. A., Volkmann, T. H. M., Wang, Y., Troch, P. A., and J., H. C.: The mechanistic basis for storage-dependent age distributions of water discharged from an experimental hillslope, Water Resour. Res., 53, 2733–2754, https://doi.org/10.1002/2016WR019901, 2017.

Queloz, P., Carraro, L., Benettin, P., Botter, G., Rinaldo, A., and Bertuzzo, E.: Transport of fluorobenzoate tracers in a vegetated hydrologic control volume: 2. Theoretical inferences and modeling., Water Resour. Res, 51, 2793–2806, https://doi.org/10.1002/2014WR016508, 2015.

Rinaldo, A. and Marani, M.: Basin Scale Model of Solute Transport, Water Resour. Res., 23, 2107–2118, https://doi.org/10.1029/WR023i011p02107, 1987.

Rinaldo, A., Botter, G., Bertuzzo, E., Uccelli, A., Settin, T., and Marani, M.: Transport at basin scales: 1. Theoretical framework, Hydrol. Earth Syst. Sci., 10, 19–29, https://doi.org/10.5194/hess-10-19-2006, 2006.

Rinaldo, A., Benettin, P., Harman, C. J., Hrachowitz, M., McGuire, K. J., van der Velde, Y., et al.: Storage selection functions: A coherent framework for quantifying how catchments store and release water and solutes, Water Resour. Res., 51, 4840–4847, https://doi.org/10.1002/2015WR017273, 2015.

Rodriguez, N. B., McGuire, K. J., and Klaus, J.: Time-Varying Storage–Water Age Relationships in a Catchment With a Mediterranean Climate, Water Resour. Res., 54, 3988–4008, https://doi.org/10.1029/2017WR021964, 2018.

Rodriguez, N. B., Pfister, L., Zehe, E., and Klaus, J.: A comparison of catchment travel times and storage deduced from deuterium and tritium tracers using StorAge Selection functions, Hydrol. Earth Syst. Sci., 25, 401–428, https://doi.org/10.5194/hess-25-401-2021, 2021.

Rodríguez-Cruz, M. S., Jones, J. E., and Bending, G. D.: Field-scale study of the variability in pesticide biodegradation with soil depth and its relationship with soil characteristics, Soil Biology and Biochemistry, 38, 2910–2918, https://doi.org/10.1016/j.soilbio.2006.04.051, 2006.

Samaniego, L., Kumar, R., and Attinger, S.: Multiscale parameter regionalization of a grid-based hydrologic model at the mesoscale, Water Resour. Res., 46, W05 523, https://doi.org/10.1029/2008WR007327, 2010.

Schoups, G., van de Giesen, N. C., and Savenije, H. H. G.: Model complexity control for hydrologic prediction, Water Resour. Res., 44, W00B03, https://doi.org/10.1029/2008WR006836, 2008.

Seeger, S. and Weiler, M.: Reevaluation of transit time distributions, mean transit times and their relation to catchment topography, Hydrol. Earth Syst. Sci., 18, 4751–4771, https://doi.org/10.5194/hess-18-4751-2014, 2014.

Soulsby, C. and Tetzlaff, D.: Towards simple approaches for mean residence time estimation in ungauged basins using tracers and soil distributions, J. Hydrol., 363, 60–74, https://doi.org/10.1016/j.jhydrol.2008.10.001, 2008.

Soulsby, C., Tetzlaff, D., Rodgers, P., Dunn, S., and Waldron, S.: Runoff processes, stream water residence times and controlling landscape characteristics in a mesoscale catchment: An initial evaluation, J. Hydrol., 325, 197–221, https://doi.org/10.1016/j.jhydrol.2005.10.024, 2006.

Stewart, M. K., Morgenstern, U., and McDonnell, J. J.: Truncation of stream residence time: How the use of stable isotopes has skewed our concept of streamwater age and origin, Hydrol. Process., 24, 1646–1659, https://doi.org/10.1002/hyp.7576, 2010.

Stewart, M. K., Morgenstern, U., McDonnell, J. J., and Pfister, L.: The 'hidden streamflow' challenge in catchment hydrology: A call to action for stream water transit time analysis, Hydrol. Process., 26, 2061–2066, https://doi.org/10.1002/hyp.9262, 2012.

Stockinger, M. P., Lücke, A., McDonnell, J. J., Diekkrüger, B., Vereecken, H., and Bogena, H. R.: Interception effects on stable isotope driven streamwater transit time estimates, Geophys. Res. Lett., 42, 5299–5308, https://doi.org/doi:10.1002/2015GL064622, 2015.

Stockinger, M. P., Bogena, H. R., Lücke, A., Diekkrüger, B., Cornelissen, T., and Vereecken, H.: Tracer sampling frequency influences estimates of young water fraction and streamwater transit time distribution, J. Hydrol., 541, 952–964, https://doi.org/10.1016/j.jhydrol.2016.08.007, 2016.

Sutanudjaja, E. H., Van Beek, R., Wanders, N., Wada, Y., Bosmans, J. H. C., et al.: PCR-GLOBWB 2: a 5 arcmin global hydrological and water resources model, Geosci. Model Dev., 11, 2429–2453, https://doi.org/10.5194/gmd-11-2429-2018, 2018.

Svensson, T., Lovett, G. M., and Likens, G. E.: Is chloride a conservative ion in forest ecosystems?, Biogeochemistry, 107, 125–134, https://doi.org/10.1007/s10533-010-9538-y, 2012.

Tetzlaff, D., Piovano, T., A., P., Smith, A., K., C. S., Marsh, P., Wookey, P. A., Street, L. E., and Soulsby, C.: Using stable isotopes to estimate travel times in a data-sparse Arctic catchment: Challenges and possible solutions, Hydrol. Process., 32, 1936–1952, https://doi.org/10.1002/hyp.13146, 2018.

Thiemig, V., Rojas, R., Zombrano-Bigiarini, M., and De Roo, A.: Hydrological evaluation of satellite-based rainfall estimates over the Volta and Baro-Akobo Basin, J. Hydrol., 499, 324–338, https://doi.org/10.1016/j.jhydrol.2013.07.012, 2013.

Timbe, E., Windhorst, W., Celleri, R., Timbe, L., Crespo, R., Frede, H. G., Feyen, J., and Breuer, L.: Sampling frequency trade-offs in the assessment of mean transit times of tropical montane catchment waters under semi-steady-state conditions, Hydrol. Earth Syst. Sci., 19, 1153–1168, https://doi.org/10.5194/hess-19-1153-2015, 2015.

Van der Velde, Y., De Rooij, G. H., Rozemeijer, J. C., Van Geer, F. C., and Broers, H. P.: Nitrate response of a lowland catchment: On the relation between stream concentration and travel time distribution dynamics, Water Resour. Res., 46, W11 534, https://doi.org/10.1029/2010WR009105, 2010.

van der Velde, Y., Torfs, P. J. J. F., van der Zee, S. E. A. T. M., and Uijlenhoet, R.: Quantifying catchment-scale mixing and its effect on time-varying travel time distributions, Water Resour. Res., 48, W06 536, https://doi.org/10.1029/2011WR011310, 2012.

Van Meter, K. J., Basu, N. B., and Van Cappellen, P.: Two centuries of nitrogen dynamics: legacy sources and sinks in the Mississippi and Susquehanna river basins, Global Biogeochemical Cycles, 31, 2–23, https://doi.org/10.1002/2016GB005498, 2017.

Visser, A., Broers, H. P., Purtschert, R., Sültenfuß, J., and de Jonge, M.: Groundwater age distributions at a public drinking water supply well field derived from multiple age tracers (85Kr, 3H/3He, and 39Ar), Water Resour. Res., 49, 7778–7796, https://doi.org/10.1002/2013WR014012, 2013.

Visser, A., Thaw, M., Deinhart, A., Bibby, R., Safeeq, M., Conklin, M., Esser, B., and van der Velde, Y.: Cosmogenic isotopes unravel the hydrochronology and water storage dynamics of the Southern Sierra critical zone, Water Resour. Res., 55, 1429–1450, https://doi.org/10.1029/2018WR023665, 2019.

von Freyberg, J., Studer, B., and Kirchner, J. W.: A lab in the field: high-frequency analysis of water quality and stable isotopes in stream water and precipitation, Hydrol. Earth Syst. Sci., 21, 1721–1739, https://doi.org/10.5194/hess-21-1721-2017, 2017.

von Freyberg, J., Allen, S. T., Seeger, S., Weiler, M., and Kirchner, J. W.: Sensitivity of young water fractions to hydro-climatic forcing and landscape properties across 22 Swiss catchments, Hydrol. Earth Syst. Sci., 22, 3841–3861, https://doi.org/10.5194/hess-22-3841-2018, 2018.

von Freyberg, J., Rücker, A., Zappa, M., Schlumpf, A., Studer, B., and Kirchner, J. W.: Four years of daily stable water isotope data in stream water and precipitation from three Swiss catchments, Sci Data, 9, 46, https://doi.org/10.1038/s41597-022-01148-1, 2022.

Wang, S., Hrachowitz, M., Schoups, G., and Stumpp, C.: Stable water isotopes and tritium tracers tell the same tale: No evidence for underestimation of catchment transit times inferred by stable isotopes in SAS function models, Hydrol. Earth Syst. Sci. Discuss. [preprint], in review, https://doi.org/10.5194/hess-2022-400, 2022.

Wilusz, D. C., Harman, C. J., and Ball, W. P.: Sensitivity of Catchment Transit Times to Rainfall Variability Under Present and Future Climates, Water Resour. Res., 53, 10 231–10 256, https://doi.org/10.1002/2017WR020894, 2017.

Wilusz, D. C., Harman, C. J., Ball, W. P., Maxwell, R. M., and Buda, A. R.: Using Particle Tracking to Understand Flow Paths, Age Distributions, and the Paradoxical Origins of the Inverse Storage Effect in an Experimental Catchment, Water Resour. Res., 56, e2019WR025 140, https://doi.org/10.1029/2019WR025140, 2020.

Winter, C., Lutz, S. R., Musolff, A., Kumar, R. Weber, M., and Fleckenstein, J. H.: Disentangling the Impact of Catchment Heterogeneity on Nitrate Export Dynamics From Event to Long-Term Time Scales, Water Resour. Res., 57, e2020WR027 992, https://doi.org/10.1029/2020WR027992, 2020.

Wollschläger, U., Attinger, S., Borchardt, D., Brauns, M., Cuntz, M., Dietrich, P., et al.: The Bode hydrological observatory: a platform for integrated, interdisciplinary hydro-ecological research within the TERENO Harz/Central German Lowland Observatory, Environmental Earth Sciences, 76, 29, https://doi.org/10.1007/s12665-016-6327-5, 2017.

Xu, G., Magen, H., Tarchitzky, J., and Kafkafi, U.: Advances in Chloride Nutrition of Plants, Adv. Agron., 68, 97–150, https://doi.org/10.1016/S0065-2113(08)60844-5, 1999.

Zink, M., Kumar, R., Cuntz, M., and Samaniego, L.: A high-resolution dataset of water fluxes and states for Germany accounting for parametric uncertainty, Hydrol. Earth Syst. Sci., 21, 1769–1790, https://doi.org/10.5194/hess-21-1769-2017, 2017.